Bioactive Materials 13 (2022) 300–311

Contents lists available at ScienceDirect

Bioactive Materials

journal homepage: www.keaipublishing.com/en/journals/bioactive-materials

Exosomal PD-L1 induces osteogenic differentiation and promotes fracture healing by acting as an immunosuppressant

Ze Lin [a,b,1], Yuan Xiong [a,b,1], Weilin Meng [c,1], Yiqiang Hu [a,b,1], Lili Chen [b,g], Lang Chen [a,b], Hang Xue [a,b], Adriana C. Panayi [d], Wu Zhou [a,b], Yun Sun [e], Faqi Cao [a,b], Guodong Liu [f], Liangcong Hu [a,b], Chenchen Yan [a,b], Xudong Xie [a,b], Chuanchuan Lin [c], Kaiyong Cai [c], Qian Feng [c,***], Bobin Mi [a,b,**], Guohui Liu [a,b,*]

[a] Department of Orthopaedics, Union Hospital, Tongji Medical College, Huazhong University of Science and Technology, Wuhan, 430022, China
[b] Hubei Province Key Laboratory of Oral and Maxillofacial Development and Regeneration, Wuhan, 430022, China
[c] Key Laboratory of Biorheological Science and Technology, Ministry of Education, College of Bioengineering, Chongqing University, Chongqing, 400044, China
[d] Division of Plastic Surgery, Brigham and Women's Hospital, Harvard Medical School, Boston, MA, 02152, USA
[e] Department of Neurosurgery, Union Hospital, Tongji Medical College, Huazhong University of Science and Technology, Wuhan, 430022, China
[f] Medical Center of Trauma and War Injuries, Daping Hospital, Army Medical University, Chongqing, 400042, China
[g] Department of Stomatology, Union Hospital, Tongji Medical College, Huazhong University of Science and Technology, Wuhan, 430022, China

ARTICLE INFO

Keywords:
PD-L1
Exosome
Fracture healing
Hydrogel
Immunotherapy

ABSTRACT

A moderate inflammatory response at the early stages of fracture healing is necessary for callus formation. Over-active and continuous inflammation, however, impairs fracture healing and leads to excessive tissue damage. Adequate fracture healing could be promoted through suppression of local over-active immune cells in the fracture site. In the present study, we achieved an enriched concentration of PD-L1 from exosomes (Exos) of a genetically engineered Human Umbilical Vein Endothelial Cell (HUVECs), and demonstrated that exosomes overexpressing PD-L1 specifically bind to PD-1 on the T cell surface, suppressing the activation of T cells. Furthermore, exosomal PD-L1 induced Mesenchymal Stem Cells (MSCs) towards osteogenic differentiation when pre-cultured with T cells. Moreover, embedding of Exos into an injectable hydrogel allowed Exos delivery to the surrounding microenvironment in a time-released manner. Additionally, exosomal PD-L1, embedded in a hydrogel, markedly promoted callus formation and fracture healing in a murine model at the early over-active inflammation phase. Importantly, our results suggested that activation of T cells in the peripheral lymphatic tissues was inhibited after local administration of PD-L1-enriched Exos to the fracture sites, while T cells in distant immune organs such as the spleen were not affected. In summary, this study provides the first example of using PD-L1-enriched Exos for bone fracture repair, and highlights the potential of Hydrogel@Exos systems for bone fracture therapy through immune inhibitory effects.

1. Introduction

Bone fracture healing is a complicated repair process, with impaired healing having a significant impact on quality of life. With 5–10% of bone fracture patients suffering from delayed healing or non-union, this is a severe global public health issue that needs to be addressed [1–3]. Although a variety of advanced therapeutic strategies for bone non-union have been developed, the benefits are not as extensive as expected [4,5]. At the early stages of bone fracture healing, inflammatory cells and immune cells recruited from neighboring areas or the circulation are gathered at the fracture site. The complement, coagulation components and cytokines produced by these cells help eliminate

Peer review under responsibility of KeAi Communications Co., Ltd.
* Corresponding author. Department of Orthopaedics, Union Hospital, Tongji Medical College, Huazhong University of Science and Technology.
** Corresponding author. Department of Orthopaedics, Union Hospital, Tongji Medical College, Huazhong University of Science and Technology.
*** Corresponding author. College of Bioengineering Chongqing University, Chongqing, 400044, China.
E-mail addresses: qianfeng@cqu.edu.cn (Q. Feng), mibobin@hust.edu.cn (B. Mi), liuguohui@hust.edu.cn (G. Liu).
[1] Co-first author: Ze Lin, Yuan Xiong, Weilin Meng, and Yiqiang Hu contributed equally to this work.

https://doi.org/10.1016/j.bioactmat.2021.10.042
Received 2 August 2021; Received in revised form 27 October 2021; Accepted 28 October 2021
Available online 3 November 2021

cell debris and bacteria [6,7]. A moderate inflammatory response at the early stage of fracture repair is imperative for proper bone healing. However, over-active and continuous inflammation after bone injury leads to impaired fracture healing. Therefore, suppression of overactive immune cells to the fracture sites may be a promising therapy for bone fractures [1,8,9].

Exosomes (Exos), membrane vesicles secreted by a wide array of cells, have gained significant scientific and clinical interest [10–12]. Studies have reported that Exos perform multiple roles in tissue regeneration, mediating the development of pathological tissue regeneration [13]. Prior studies have reported the potential mechanisms of Exos in the inhibition of an overactive immune response [14]. The ability of Exos to suppress the function of $CD8^+$ T cells and natural killer cells (NKs), hinder the maturation of dendritic cells (DCs), and promote the activity of regulatory T cells (Tregs) is well documented [15–17]. Thus, Exos have great potential to act as effective factors in the regulation of the immune response and tissue regeneration.

Promoting the proliferation of antigen-specific T cells is a reaction of the immune system against foreign antigens that accumulate in the lymph nodes or spleen [18]. Programmed cell death ligand 1 (PD-L1) is a protein which can cross the cell membrane [19]. PD-L1, as the ligand of Programmed Cell Death Receptor-1 (PD-1), specifically binds to PD-1 and transmits inhibitory signal transduction to suppress the T cells proliferation [20,21]. The expression of PD-L1 is trigged by pro-inflammatory factors in various cells, which could be specifically coupled to the PD-1 of T lymphocytes, suppressing the immune recognition function of T lymphocytes [22]. Consequently, PD-L1 may be a promising target in conditions related to an overactive immune response. Interestingly, recent research has suggested that HUVECs can inhibit the Tregs activation via modulation of PD-L1 expression [23]. Exos derived from HUVECs have the potential to induce bone remodeling in a bone-targeted manner [24]. Furthermore, a recent study has shown that HUVEC-derived exosomes with high expression of PDL1 can effectively inhibit the inflammatory response at the wound [25]. However, few studies have focused on the role of PD-L1 in fracture repair. Thus, we set out to investigate if a high concentration of PD-L1 can be obtained from Exos from genetically engineered HUVECs, and whether exosomal PD-L1 is able to modulate the inflammatory and immune response in order to provide adequate immune homoeostasis during bone remodeling.

In the present study, Exosomal PD-L1 was obtained from genetically engineered HUVECs, which could overexpress PD-L1. Our results suggested that exosomal PD-L1 was capable of inhibiting T cell proliferation, and consequently induced MSCs towards osteogenic differentiation *in vitro*, and promoted fracture healing *in vivo*. Furthermore, our results suggested that sustained release of exosomal PD-L1 from the hydrogel led to decrease of $CD8^+$ T lymphocyte in nearby peripheral lymph nodes, but not $CD8^+$ T lymphocyte in spleen of the murine fracture model during the inflammatory phase. Our results indicate a new immunosuppressive effect of exosomal PD-L1 and offer the first example of using PD-L1-enriched Exos for bone regeneration (Scheme 1).

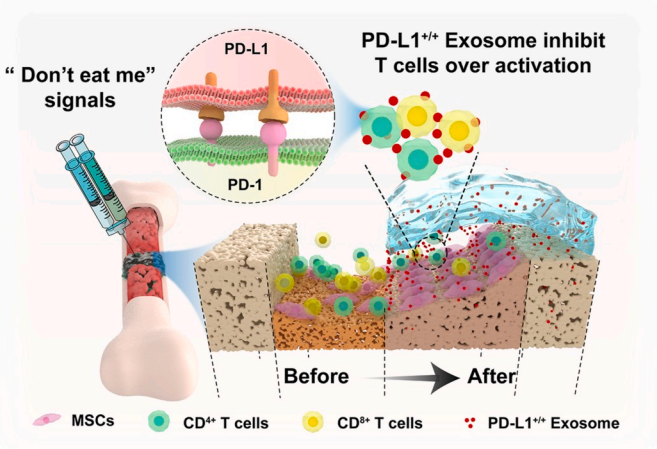

Scheme 1. Schematic illustration of therapeutic process for fracture healing by using exosomal PD-L1. The Exos with high concentration of PD-L1 is slowly released from the HA/Gel hydrogel, binds to PD-1 on the T cell membrane at fracture site and triggers the immune checkpoint mechanism, and thereby suppressing over-active inflammation and promoting fracture healing.

2. Materials and methods

2.1. Synthesis of oxidized hyaluronic acid (HA-CHO)

First, 2 g of Sodium hyaluronate (Shandong Focusfreda Biotech Co., China) was dissolved in 200 mL deionized water (DI water). The solution was stirred for 24 h in the dark after addition of 1.2 g of $NaIO_4$ (Aladdin, China). The resulting solution was purified by dialysis (MWCO: 8–14 kDa) against DI water for four days. In the end,the solution was lyophilized for three days and kept in a desiccator under 4 °C until use.

2.2. Synthesis of hydrazide grafted gelatin(Gel-ADH)

First, 2 g gelatin was dissolved in 200 mL Morpholine ethanesulfonic acid (MES, J&K Scientific) solution (0.5 w/v%, pH 6.5). Then, 2.3012 g of Adipic acid dihydrazide (ADH, J&K Scientific) was added to the gelatin solution and stirred at 37 °C or 2 h. After returning to room temperature, 0.5066 g of N-(3-Dimethylaminopropyl)-N′-ethylcarbodiimide hydrochloride (EDC, J&K Scientific) and 0.357 g of 1-Hydroxybenzotriazole (HOBT, J&K Scientific) was added to the solution and stirred at room temperature for 22 h. The resulting solution was purified by dialysis (MWCO 8–14 kDa) against DI water for five days. Then, the dialyzed solution was freeze dried under vacuum to obtain yield purified product Gel-ADH.

2.3. Fabrication of the injectable HA/Gel hydrogel

The HA/Gel hydrogel was prepared *via* one-step equal volume mixing between PBS solution of HA-CHO and Gel-ADH. During the experiments, the final concentration of Gel-ADH was fixed in HA/Gel hydrogel as 16 wt%, while adjusting the final concentration of HA-CHO in hydrogel as 4 wt%, 6 wt%, and 8 wt%.

2.4. Morphology characterization

The prepared HA/Gel hydrogel was rapidly freeze with liquid nitrogen to fix its morphology before lyophilization. A scanning electron microscope (SEM) was used to cross section the HA/Gel hydrogel after uniform gold spraying.

2.5. Swelling ratio test

The swelling ratios of the developed hydrogel (n = 3) were determined gravimetrically. The prepared HA/Gel hydrogels were immersed in PBS (pH 7.2). After 24 h, the swelled hydrogels were collected to be weighted after wiping with filter paper to remove excess liquid on the sample surface and the weight was recorded as W_s. After this, the collected hydrogel samples were dried in a dryer for 24 h and weighed again and the weight was recorded as W_d. The swelling ratios were calculated using the following equation: Swelling ratio (%) = $(W_s\text{-}W_d)/W_d \times 100$.

2.6. Rheological characterization

Both the rheological time sweep and shear thinning test of the HA/Gel hydrogels was carried out with TA Discovery-2 using 20 mm diameter plates at a 3 mm gap size at 37 °C. For the time sweep test, the

strain and frequency were fixed at 1% and 1 Hz, respectively. As for the shear thinning test, the samples were sheared for 4 cycles of low (1%, 120s) – high (200%, 120s) strain under a frequency of 1 Hz.

2.7. Adhesive strength test

The adhesion property of HA/Gel hydrogels was measured by using a universal mechanics testing machine equipped with a 30 N load cell. In brief two pieces of fresh pigskins, glass or titanium were glued with 100 mL HA/Gel hydrogel and the contact area was fixed as 25 mm × 10 mm. For the whole lap shear testing, the tensile rate was kept as 0.2 mm/s.

2.8. In vitro degradation

Briefly, HA/Gel hydrogels with known weight (W_0) were soaked in three different solutions: (1) pure PBS; (2) PBS solution of 0.0025% trypsin; and (3) PBS solution of 0.01% trypsin (n = 3). At definite time points (30, 60, 90, 120 min), the weight of the HA/Gel hydrogel was recorded as W_x. The degradation rate (DR) curve was calculated using the following equation: $DR(\%)=(W_x\text{-}W_0)/W_0 \times 100$.

2.9. HUVEC culture and transfection

HUVECs were incubated with RPMI 1640, which containing 10% exosome-depleted FBS. Lipofectamine 3000 was applied for cell transfection according to the instructions. HUVECs were cultured with 95% humidity and 5% CO_2 at 37 °C. The PD-L1 plasmid and PD-L1 siRNA were constructs from GenePharma (Shanghai). The cells expressing PD-L1 ($HUVEC^{PD-L1}$) was obtained by transfected with PD-L1 plasmid (GenePharma, Shanghai). Likewise, PD-L1 in cells were detected ($HUVEC^{PD-L1-/-}$) by transfected with PD-L1 siRNA (GenePharma, Shanghai). A large number of HUVECs were transfected with the PD-L1 plasmid or siRNA, and the cell supernatant was collected within 48 h after successful transfection for the extraction of exosomes. This was to minimize reduction of the siRNA or plasmid.

2.10. Exos isolation and identification

Cell supernatant was collected into centrifuge tubes and centrifuged at 3000×*g* for 15 min. Centrifuged again to remove remaining cell fragments. The supernatant was centrifuged at 10,000×*g* for half an hour, followed by ultracentrifuged at 100,000×*g* for 70 min. Exos were washed with phosphate buffered saline (PBS) for three times, then ultracentrifuged at 100,000×*g* for another 70 min. The Exos were then re-suspended in PBS and filtered with a 0.2 μm filter. Next, Exos were ultrafiltered with a 15 mL Centrifugal Filter by centrifugated at 4 000×*g*. Next, the purified Exos were mixed with 4% osmium tetroxide at 4 °C for 30 min, and then submitted to the copper grid, which were stained with 1% phosphotungstic acid. Morphology was assessed by TEM (EFI, TECNAI G2). The Dynamic Light Scattering (DLS) was evaluated by a Nanosizer instrument, and the marker proteins expression of Exos surface by western blotting.

2.11. Western blot

The cell samples were lysed by buffer containing 1% protease inhibitor (Aspen). The SDS-PAGE-separated protein samples were then transferred to NC membranes (Millipore). Afterwards, NC membranes blocked with 5% skim milk and then incubated at 4 °C overnight with homologous primary antibodies for collagen I, ALP, OCN, and β-actin (Abcam, UK) . Blots were incubated with secondary antibodies at 4 °C for 4 h, conjugated with horseradish peroxidase (HRP, Aspen). At the end, the proteins were observed by chemiluminescence examination system.

2.12. qRT-PCR analysis

TRIzol® was applied to extract the total RNA from cells and callus. RNA was reversely transcribed into cDNA with HiScript III RT SuperMix (Vazyme, China), and quantified using 2x SYBR Green qPCR Mix. Relative mRNA expression folding alteration was calculated with the $2^{-\Delta\Delta Ct}$ approach and the primer sequences are as follow: Human PD-L1, forward, TCCACTCAATGCCTCAAT, reverse, GAAGACCTCACAGACTCAA; Human β-actin, forward, CCACACTGTGCCCATCTAC, reverse, AGGATCTTCATGAGGTAGTCAGTC; Mouse TNF-α, forward, CATCCTTGCGAGTGTCAGTGA, reverse, CCCTCACACTCAGATCATCTTCT; Mouse IL-6, forward, CCTCTGGTCTTCTGGAGTACC, reverse, ACTCCTTCTGTGACTCCAGC; Mouse Granzyme B, forward, TCTCGACCCTACATGGCCTTA, reverse, TCCTGTTCTTTGATGTTGTGGG; Mouse β-actin, forward, GGCTGTATTCCCCTCCATCG, reverse, CCAGTTGGTAACAATGCCATGT.

2.13. MSCs culture and transfection

MSCs were extracted from healthy donor's marrow. The extracted cells were stimulated and cultured in the specific media for mesenchymal stem cells (#MUXMA-90021, Cyagen) at 37 °C. Cells were cultured and used for the *in vitro* assay in three passages.

2.14. Alizarin red staining

MSCs were continuously cultured in 24-well plates in an osteogenic medium for 21 days to induce osteogenesis. MSCs were washed three times with PBS, after which 10% tissue fixative was used to fix the cells. Then, 0.5% alizarin red staining dye was applied to stain cells. And the red mineralized nodules were observed using a charge-coupled device microscope and the absorbance was evaluated at 570 nm.

2.15. ALP staining

An ALP staining kit was used for MSCs staining. MSCs were washed twice, and 10% 10% tissue fixative was used to fix the cells. BCIP/NBT substrate was applied to incubate cells for 24 h. Colorimetric alteration was calculated with a charge-coupled microscope and absorbance was evaluated at 405 nm.

2.16. Immunostaining

To visualize PD-L1 on the cell membrane or on exosomes, the GFP-PD-L1 encoding plasmid (Genechem, Shanghai) was transfected into HEK 293T cells for 6 h. PD-L1 on the cell membrane was labelled with green fluorescent. PD-L1-overexpressing exosomes ($HUVEC^{PD-L1@Exos}$, 50 μg/ml) were stained by PKH26 and excess dye was removed. Cells were cultured with PKH26-labelled Exos, followed by seeded on the top of glass coverslips. Images were collected using a confocal microscope with multiple objectives.

2.17. Lymphocyte isolation and proliferation

Lymphocytes were harvested from the C57BL/6 mouse's spleen. Firstly, the spleen was obtained under aseptic conditions, and placed on a 75 μm filter. The spleen was minced using the bottom end of a sterile syringe while simultaneously washing with PBS. The washed suspended cells were collected in a centrifuge tube. After centrifugation at 1500 rpm for 10 min, cells were resuspended in 3 ml red blood cell lysis solution, and incubated at room temperature for 10 min. After being centrifuged again, cells were washed three times with PBS. Finally, the cells were resuspended in a 1640 medium and transferred to a culture flask. After 24 h of culture, lymphocytes were obtained . Lymphocyte (1×10^6) were stained with carboxyfluorescein succinimidyl ester (CFSE, BioLegend) (5 mM). Lymphocyte were cultured with Exos (100 μg/ml)

extracted from HUVECs, HUVEC^{PD-L1} cells, and HUVEC$^{PD-L1-/-}$ cells for 4 days, respectively. As a contrast, lymphocytes were also incubated with HUVEC$^{PD-L1-/-@Exos+PD-L1}$ (100 μg/ml). Lymphocytes were stained with CFSE and incubated with 1640 culture medium for 4 days as control groups (PBS). Meanwhile, phorbol ester (PMA, 10 ng/mL) was added to the culture medium of each group, in order to stimulate lymphocyte proliferation. The proliferation of lymphocyte was assessed by flow cytometry (FCM) analysis, and T cells were labelled with antibodies of PE anti-mouse CD3 (BioLegend) to observe the proliferation of T cells.

2.18. In vitro cytotoxicity

The Calcein-AM/PI double staining kit (Sigma-Aldrich) was applied to evaluate the viability of hBMSCs seeded on hydrogels for 96 h. Fluorescence images were acquired using a microscope (IX53, Olympus, Japan).

2.19. Exos uptake by MSCs in hydrogel condition

Exos in PBS were stained with PKH26 (#MINI26-1 KT, Sigma, MO, USA). 20% HA/GEL hydrogel-containing PKH26-stained Exos (50 μg/ml) were incubated for 10 min, followed by adding to the MSCs layer. In the negative control groups, same volume of serum-free medium was used and incubated at 37 °C for 1, 4, 8, 24 and 36 h. After three washing steps, cells were stained with 4% paraformaldehyde, and the nuclei were stained with DAPI at 0.5 μg/mL for 15 min (blue), and images were captured using confocal microscopy.

2.20. Co-immunoprecipitation

After incubation with exosomes, HEK-293T cells were lysed with HC buffer (150 mM NaCl; 20 mM Tris-HCl pH 7.5; 1% NP40; 1.0 mM EDTA and protease inhibitors) and incubated on ice for 30 min. Then lysates were centrifuged at 14000 g for 10 min. The supernatant was pre-clean with A/G agarose beads (Pierce, Thermo Scientific), and incubated for 1 h at 4 °C. After centrifugation again, the magnetic beads were discarded, and the supernatant was incubated with PD-L1 antibody overnight at 4 °C. Afterwards, immune complexes were incubated with A/G agarose beads overnight at 4 °C. Finally, the immune complexes were washed 3 times and boiled at 95 °C for 5 min.

2.21. Mice fracture model

All animal experiments have obtained consent from the Institutional Animal Care and Use Committee at Tongji Medical College, Huazhong University of Science and Technology (HUST). Pentobarbital sodium (50 mg/kg) was utilized (i.p.) to anesthetize mice, then the femoral fracture model was constructed as previously reported [26]. The femur was break using a diamond disk to achieve a mid-diaphysis fracture line, and a 25-gauge intramedullary needle was inserted into the medullary cavity to provide adequate stability for the fractured bone.

2.22. Animal administration

The groups were treated with HA/Gel hydrogel alone (Control) or HA/Gel hydrogel containing HUVEC^{Exos}, HA/Gel hydrogel containing HUVEC$^{PD-L1@Exos}$, HA/Gel hydrogel containing HUVEC$^{PD-L1-/-@Exos}$ (HUVEC^{Exos}, HUVEC$^{PD-L1@Exos}$, HUVEC$^{PD-L1-/-@Exos}$ groups) injected to the fracture sites over the 21 days. Animals were treated every three days from the third day post-injury. On day seven, half of the mice were sacrificed and the formed callus, spleen and lymph nodes were collected for further analysis. The remaining mice were sacrificed and the bone tissue collected at day 21 post injury. At the same time, the blood and organ were collected for the comprehensive safety evaluation.

2.23. X-rays of the fracture mice

On days 5, 9, and 14 post injury, mice were detected by X rays with an In-Vivo FX PRO imaging system (BRUKER, Karlsruhe, Germany).

2.24. Micro-computer tomography (Micro-CT) examination

This process was performed as a prior study [25]. Briefly, the micro-CT system (BRUKER 1276, Karlsruhe) was taken to capture pictures of femur fracture. The own software was applied to evaluate segmentation, construct 3-dimensional morphometric pictures, and analyze related parameters, including total volume (TV), bone volume (BV), BV/TV, bone mineral density (BMD).

2.25. Histological analysis

Following micro-CT analysis, femurs were fixed with 4% paraformaldehyde overnight and demineralized for two weeks. 7 μm paraffin-embedded tissue samples were subjected to Alcian Blue/hematoxylin-eosin (HE)/orange G staining as previously described [27].

2.26. FCM analysis

To calculate the CD8 (+) and CD4 (+) T cell ratio in the lymph nodes and mouse spleen during fracture repair, the lymph nodes and spleen were collected in a sterile environment and gilter on a 0.75-μm sieve. Cells were cultured by antibodies of APC anti-mouse CD4, CD8, and CD3 and finally evaluated using FCM analysis.

2.27. Statistical analysis

Data were displayed as mean ± standard deviation (SD). Statistical analysis was performed using Student's *t*-test (two groups) or ANOVA with Tukey's post hoc test (over two groups). Significance was considered when $p < 0.05$.

3. Results

3.1. PD-L1 enriched in HUVEC$^{PD-L1@Exos}$

To verify whether overexpression or knockout of PD-L1 in HUVECs affects the secretion of PD-L1 in Exos, we transfected the HUVECs with PD-L1 plasmid (HUVEC^{PD-L1}) or PD-L1 siRNA (HUVEC$^{PD-L1-/-}$) to obtain exosomes. The DLS analysis indicated that Exos from HUVECs, HUVEC^{PD-L1}, and HUVEC$^{PD-L1-/-}$ have a similar size distribution (40–150 nm) (Fig. 1A). Next, the TEM results showed that the obtained nanosized vesicles were membrane-bounded and round-shaped (Fig. 1B). Furthermore, we purified Exos from the constructed cells and tested the presence of PD-L1 protein and exosomal markers CD81 and TSG 101 in these Exos (Fig. 1C). Moreover, the qRT-PCR results suggested a marked increase of PD-L1 level in HUVEC^{PD-L1} and a marked decrease of PD-L1 level in HUVEC$^{PD-L1-/-}$ compared to the non-treated HUVECs (Fig. 1D).

3.2. Exosomal PD-L1 suppressed the activation of T cells, enhanced osteogenic differentiation

To check if PD-L1-overexpressing Exos were capable of interacting with PD-1 on the cell surface, HUVEC$^{PD-L1@Exos}$ were firstly stained with PKH26 dye to show the existence as small-red dots. Expectably, colocalized of pre-stained HUVEC$^{PD-L1@Exos}$ and exogenous GFP-PD-1 on the cell surface of HEK 293T cells (Fig. 2A). The results of co-immunoprecipitation also clarified the interaction (Fig. 2B). In tumor microenvironment, it is well-documented that exosomal PD-L1 is closely associated with the immunosuppression [28,29]. Thus, we then checked whether exosomal PD-L1 was capable of acting similarly as

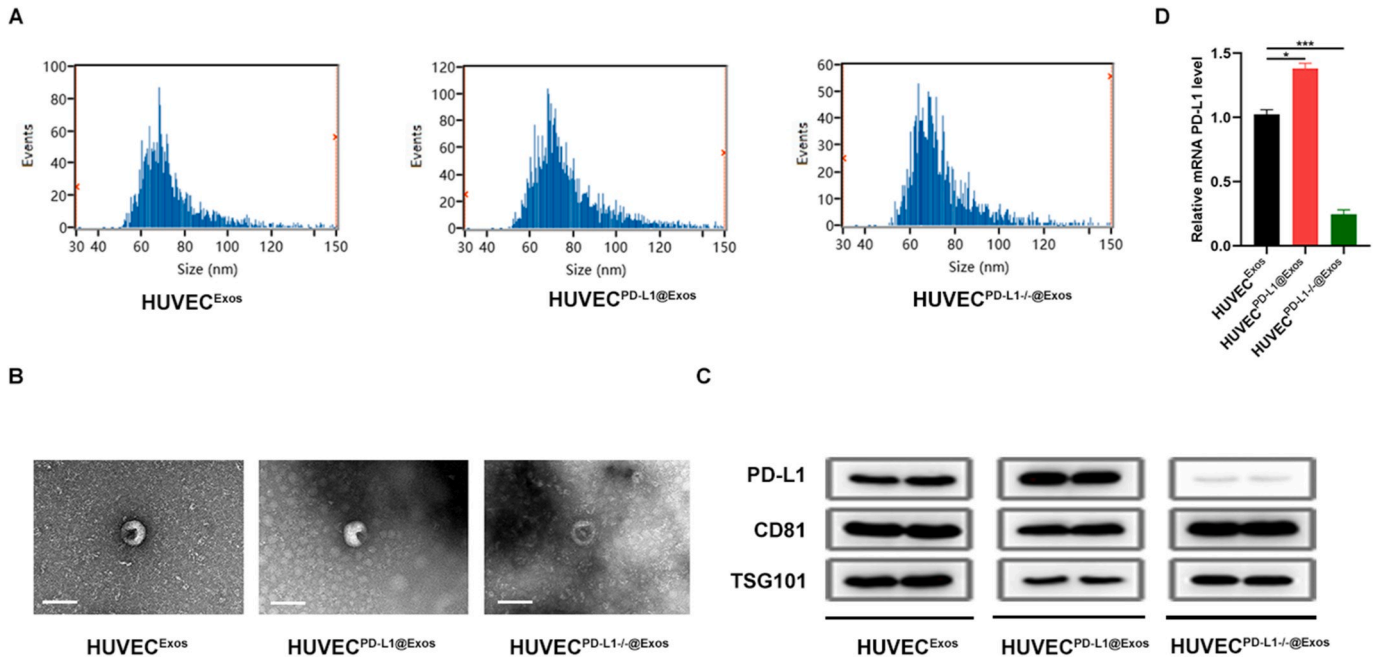

Fig. 1. Isolation and characterization of Exos from culture supernatant of HUVECs, PD-L1 overexpressed HUVECs, and PD-L1 knockout HUVECs. (A) The size distribution of $HUVEC^{@Exos}$, $HUVEC^{PD-L1@Exos}$ and $HUVEC^{PD-L1-/-@Exos}$ was measured DLS. (B) Represent image of the three kinds of Exos were achieved by TEM. Scale Bar: 100 nm. (C) The protein levels of PD-L1, CD81 and TSG101 in these kinds of exosomes. (D) The PD-L1 expression in each group was measured by qRT-PCR analysis. *P < 0.05; **P < 0.01, ***P < 0.001.

cell-surface PD-L1 in inhibition of T cell function. Our data demonstrated that $HUVEC^{PD-L1@Exos}$ and $HUVEC^{PD-L1-/-@Exos}$+PD-L1 significantly suppressed the proliferation of lymphocyte compared with $HUVEC^{PD-L1-/-@Exos}$, as confirmed by the reduced ratio of cells containing CFSE dye (Fig. 2C; Fig. S1). This result provides supporting evidence that the immune-suppression of Exos was contributed by PD-L1 rather than other proteins in Exos. Furthermore, to investigate whether this T cell suppression would affect fracture healing, we performed *in vitro* assays of MSCs by exploring conditional medium isolated from $HUVEC^{Exos}$, $HUVEC^{PD-L1@Exos}$, $HUVEC^{PD-L1-/-@Exos}$, $HUVEC^{PD-L1-/-@Exos}$+PD-L1 incubated with lymphocyte for 96 h. As shown in Fig. 2D, the osteogenic-related markers were significantly enriched in $HUVEC^{PD-L1@Exos}$ and $HUVEC^{PD-L1-/-@Exos}$+PD-L1 -treated groups compared with the PBS and $HUVEC^{PD-L1-/-@Exos}$--treated groups. Interestingly, when adding exogenous PD-L1 to the $HUVEC^{PD-L1-/-@Exos}$, the osteogenic-related markers could be partially reversed. In addition, to study the impact of exosomal PD-L1 on extracellular matrix mineralization, MSCs among the different groups were continuously cultured for 7 or 21 days, then stained with ALP or alizarin red, indicating enhanced mineral deposition in $HUVEC^{PD-L1@Exos}$ and $HUVEC^{PD-L1-/-@Exos}$+PD-L1-treated groups, and the most prominent enhanced mineral deposition was in $HUVEC^{PD-L1@Exos}$-treated group (Fig. 2E–F).

3.3. Preparation and characterization of HA/Gel hydrogel

To guarantee delivery efficiency of Exos to the bone fracture, we designed an injectable hydrogel based on natural polymer hyaluronic acid (HA) and gelatin (Gel) as the Exos carrier. We successfully synthesized oxidized hyaluronic acid (HA-CHO) and hydrazide grafted gelatin (Gel-ADH; Fig. S2). Then, the hydrogel carrier for Exos could be easily formed by equal volume mixing with HA-CHO solution and Gel-ADH solution *via* dual syringe as shown in Fig. 3A. The fast gelation of our HA/Gel hydrogel is due to the fast Schiff base reaction between the aldehyde groups of HA-CHO and hydrazide groups of Gel-ADH. In the following test, we carefully explored the influence of HA-CHO concentration on the prepared HA/Gel hydrogel. The SEM micrographs of the HA/Gel hydrogel cross section showed that all three groups of HA/Gel hydrogel had interconnected porous structure, while a higher concentration of HA-CHO could lead to a denser pore distribution (Fig. 3B). We believed that these connected pores were appropriate for the loaded Exos releasing. The swelling ratio measurements (Fig. 3C) showed that increasing the HA-CHO concentration resulted in a decrease of the swelling ratio of HA/Gel hydrogel. This data should be consistent with our SEM results, as the dense pore structure hindered water absorption. As for the rheological mechanical test (Fig. 3D) demonstrated that the HA-CHO concentration had no significant impact on the modulus of the HA/Gel hydrogel. Therefore, the high swelling ratio of the hydrogel was favorable for the absorption of exudate and guarantied effective filling of the defect while the rheological modulus of our HA/Gel hydrogel was not affected by increasing the HA-CHO concentration.

Based on this we selected the HA/Gel hydrogel (4% HA-CHO and 16% Gel-ADH) as the Exos carrier for all subsequent experiments. We observed shear-thinning property of the HA/Gel hydrogel. Fig. 3E displays that the HA/Gel hydrogel could switch between “Sol” (high strain: 200%, G’ > G’’) and “Gel” (low strain: 1%, G’ > G’’) circularly, demonstrating the dynamic balance between the break and reform of the reversible hydrazone crosslinking inside the HA/Gel hydrogel. Therefore, the HA/Gel hydrogel had a good self-healing property (Fig. 4A). As shown in Fig. 4A, two independent wing-shaped HA/Gel hydrogels could be reassembled into a new whole hydrogel after cutting. Moreover, the HA/Gel hydrogel showed good adhesion strength in different materials, especially for tissue (pigskin as the model tissue) (Fig. 4C and 4D). This excellent bio-adhesive property was due to the reaction of the aldehyde groups in HA/Gel hydrogel and the native amino groups of tissue. We believed that the rapid self-healing property and good bio-adhesive property should help our HA/Gel hydrogel carrier adhere to the surrounding native bone tissue and then maintain integrity after filling the bone defects to support Exos releasing and bone repair. In addition, the degradation property of HA/Gel hydrogel was also tested. Gelatin is a natural polymer that is degradable-sensitive to matrixmetalloproteinase (MMP). Previous studies have shown that the function of

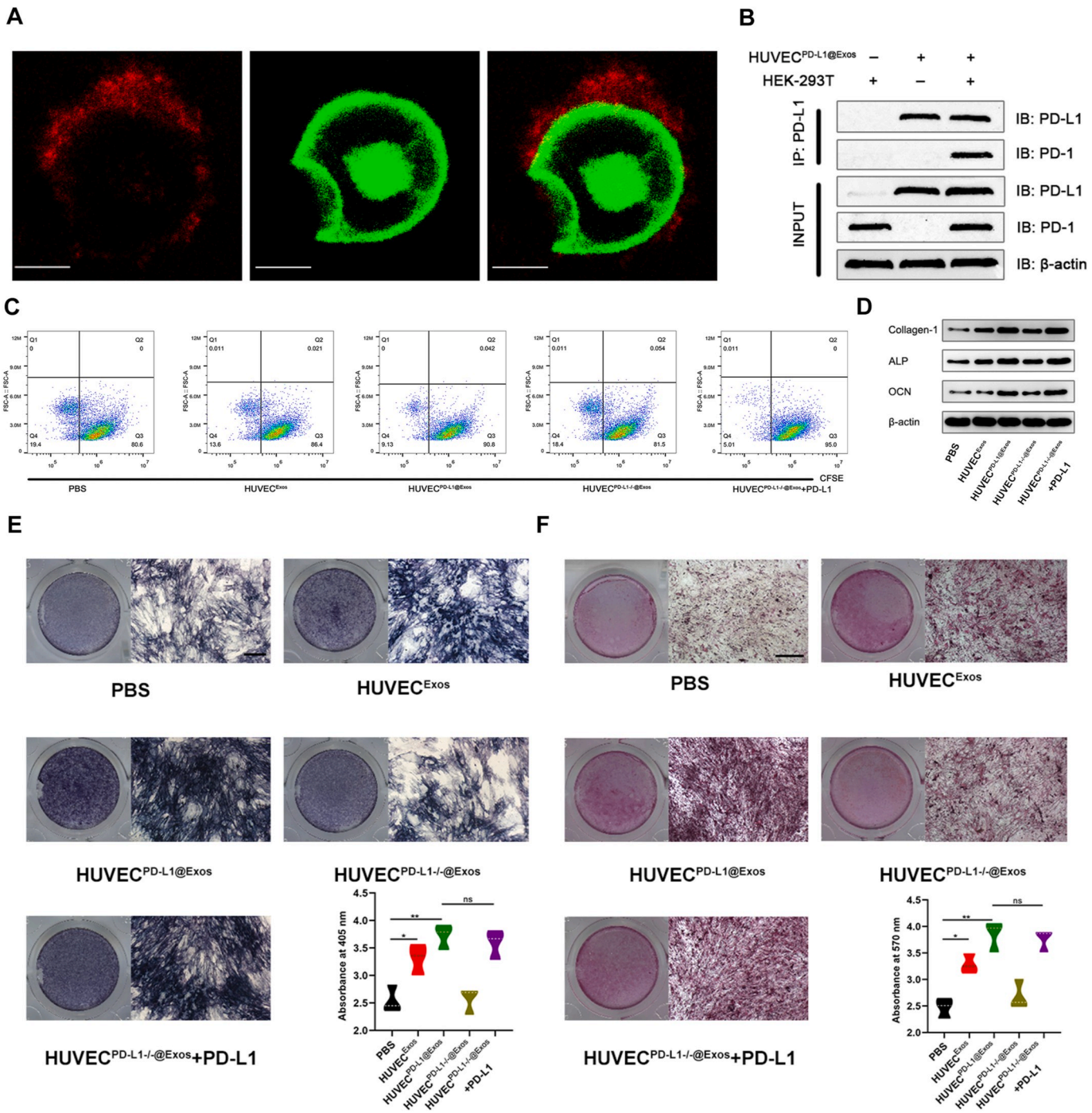

Fig. 2. Exosomal PD-L1 inhibited T cell activation and enhanced osteogenic differentiation *in vitro*. (A) Exos were labelled red fluorescence by stained with PKH26. Exos (red) colocalized with PD-1 (green) on the cell membrane of HEK-293T were observed by confocal. Scale bar: 10 μm. (B) Co-IP experiments show that PD-L1 in Exos binds PD-1 on the HEK-293T cells, PD-1 is captured by PD-L1 antibody due to the interaction with PD-L1. (C) CFSE-labelled T cell proliferation was observed by FCM analysis. Proliferating cells were observed to divide and halve the fluorescence intensity. (D) The osteogenic protein was measured by western blot. (E) ALP staining in BMSCs following treated by PBS, HUVEC$^{@Exos}$, HUVEC$^{PD-L1@Exos}$, HUVEC$^{PD-L1-/-@Exos}$ and HUVEC$^{PD-L1-/-@Exos}$+PD-L1 for 7 days. Scale bar: 10 mm. (F) Alizarin red staining in BMSCs following treated by PBS, HUVEC$^{@Exos}$, HUVEC$^{PD-L1@Exos}$, HUVEC$^{PD-L1-/-@Exos}$ and HUVEC$^{PD-L1-/-@Exos}$+PD-L1 for 21 days. Scale bar: 10 mm *P < 0.05; **P < 0.01.

trypsin and MMP is similar in some extent, so we chose easily acquired trypsin to teste the enzyme-sensitivity of our HA/Gel hydrogel degradation. Fig. 4E shows that even a low concentration of trypsin could significantly increase the degradation rate of the HA/Gel hydrogel. Therefore, we speculated that in the beginning of the bone defect repair as the MMP, especially MMP-9 expression was higher than normal state, the HA/Gel hydrogel exhibited a faster degradation to release Exos to reach a fast control of the inflammation inside the bone defect.

3.4. Timed-release of Exos from HA/Gel hydrogel

With the aim to enhance the therapeutic effects of Exos, we embedded Exos into HA/Gel hydrogel to release Exos in a timed-release manner. Next, to check if HA/Gel hydrogel was able to enhance the

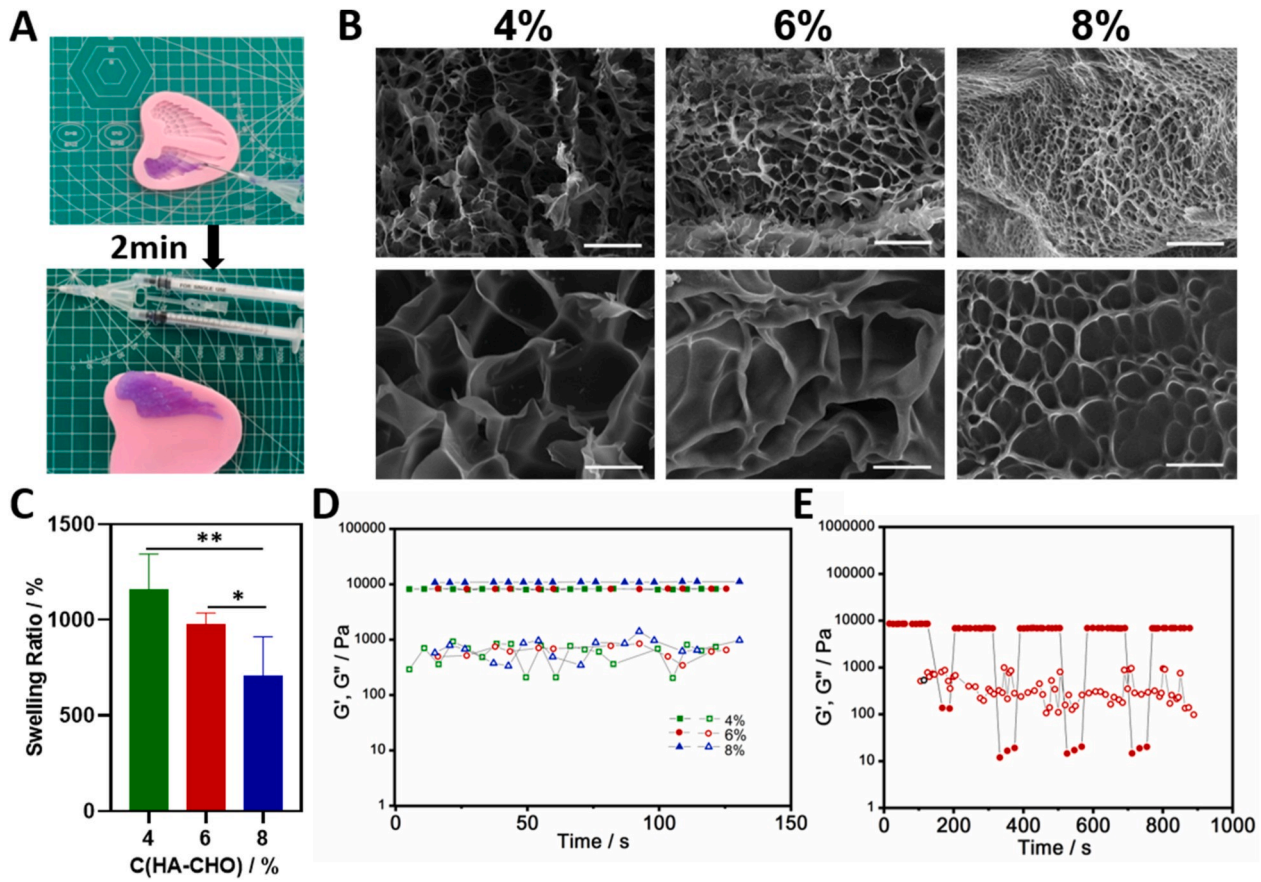

Fig. 3. The fabrication and characterization of HA/Gel hydrogel. (A) The HA/Gel hydrogel was conveniently prepared through one-step equal volume mixing *via* a dual syringe. The SEM images (B), swelling ratio analysis (C) and rheological time sweep (D) of HA/Gel hydrogels with different final concentration of HA-CHO (4%, 6%, and 8%) and fixed concentration of Gel-ADH (16%). (E) Shear tinning test of HA/Gel hydrogel (HA-CHO: 6% and Gel-ADH: 16%). The scale bar for B: 50 mm (up) and 10 mm (down). *P < 0.05; **P < 0.01. GH hydrogels exhibited a sol−gel transition during switching between alternating high (200%, G''>G′) and low (1%,G'>G'') shear strain in the rheological test at 37 °C.

stability of Exos *in vitro*, 10 μg of PKH 26-labelled Exos were incorporated in 200 μL HA/Gel hydrogel. After culturing for different time points, we evaluated the release of hydrogel-incorporated Exos by quantitating PKH26 signals. The PKH26 signal was gradually enhanced with the elongation of incubation time, and peaked after 36 h incubation (Fig. 5A–B), indicating Exos were constantly released from HA/GEL hydrogel into the surrounding cells. Furthermore, We performed a cell counting kit-8 (CCK-8) assay to examinate the viability of the cultured MSCs, finding no obvious growth difference among the experimental groups on 1, 3, 5 and 7 days after incubation. The MSCs proliferated well in the different groups, with or without hydrogel, suggesting that the applied hydrogel including HA/Gel@Exos hydrogel, was not harmful to MSCs (Fig. 5C). Moreover, cell status was checked using live/dead cell staining at 0, 3 and 5 days after culture. All the cells were morphologically similar, either in the presence of cell culture medium or hydrogel treatment (Fig. 5D–E). The H&E staining of vital organs and the detection of blood biochemical indicators was performed in a C57BL/6 mouse (Fig. 5F and Figs. S3A–C). All these results indicated a good cell viability of HA/GEL hydrogel and HA/Gel@Exos hydrogel treatments.

3.5. Exosomal PD-L1 accelerates fracture healing in mice

Based on the findings in cellular models relevant to the fracture-healing process, we investigated whether exosomal PD-L1 is a significant determinant of fracture healing. To test how exosomal PD-L1 affects fracture healing *in vivo*, we exposed different groups to different treatments. The negative group was incubated with 20% HA/GEL hydrogel alone (Control), 20% HA/GEL hydrogel containing $HUVEC^{Exos}$, 20% HA/GEL hydrogel containing $HUVEC^{PD-L1@Exos}$, as well as HA/GEL hydrogel containing $HUVEC^{PD-L1-/-@Exos}$ ($HUVEC^{Exos}$, $HUVEC^{PD-L1@Exos}$, $HUVEC^{PD-L1-/-@Exos}$ groups) were administrated to the fracture sites over the 21 days. The fractures were monitored using X-rays and micro-CT. A marked decreased fracture gap and a larger callus volume was seen in the $HUVEC^{PD-L1@Exos}$ group, compared to the $HUVEC^{PD-L1-/-@Exos}$ group. On day 21 post-fracture, the animals in the $HUVEC^{PD-L1@Exos}$ group no longer showed a clear border between hardened callus and cortical bone. However, when excluding PD-L1 from $HUVEC^{Exos}$, the beneficial effects of Exos on fracture healing were significantly hindered (Fig. 6A–B). Besides, on day 14, the mice in the $HUVEC^{PD-L1@Exos}$ group showed greater total and bone callus volume and BMD compared to the other treatments groups, remaining significant on day 21 post-injury (Fig. 6C). In addition, H&E staining on day 21 showed increased bone formation area at the fracture site when mice were treated with 20% HA/GEL hydrogel containing $HUVEC^{PD-L1@Exos}$, while removal of PD-L1 from the Exos impaired this pro-fracture-healing effect (Fig. 6D–E). These evidences demonstrated that exosomal PD-L1 effectively accelerates fracture healing in mice.

3.6. Administration of PD-L1-enriched Exos in mice exerts a local immunosuppressive effect

Finally, we examinate the immune-related cytokines in the fractured regions. The qRT-PCR and Western Bolt results suggested significantly lower level of IL-6, TNF-a, and granzyme B in the $HUVEC^{PD-L1@Exos}$ group compared to the other treatment groups (Fig. 7A–D). Consistently, FCM analysis and immunohistochemical staining suggested fewer CD8

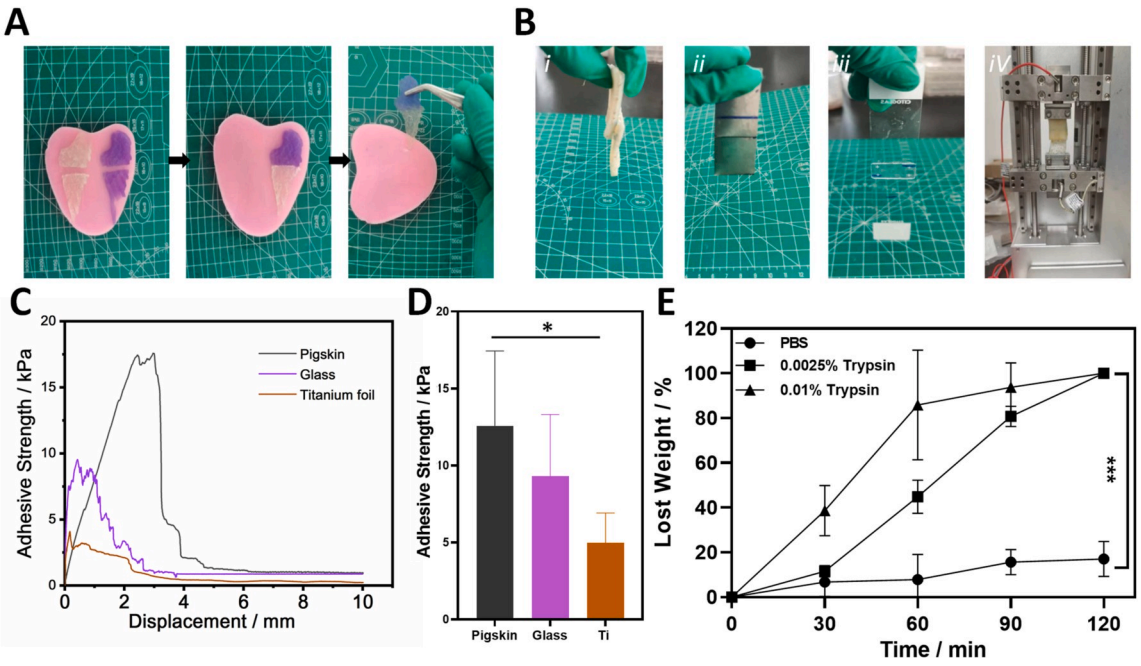

Fig. 4. The self-healing, adhesive, and enzyme-sensitive degradable properties of HA/Gel hydrogel. (A) Photographs of HA/Gel hydrogel's macroscopic self-healing performance under room temperature. (B) Images of HA/Gel hydrogel tightly glued to two pieces of pigskin(*i*), Glass (*ii*) and Titanium (*iii*), respectively and the image of lap shear test using pigskin (*iv*). (C) The lap-shear curves of HA/Gel hydrogel. (D) Adhesion strengths of HA/Gel hydrogel for different materials (n = 3). (E) Time-dependent profile of weight lose of HA/Gel hydrogel *in vitro* under different trypsin concentrations. ***P < 0.001.

(+) T cells in the lymph nodes and callus, but not observed in the spleens in the HUVEC$^{PD-L1@Exos}$ group when compared to the control and HUVEC$^{PD-L1-/-@Exos}$ groups, indicating that local administration of PD-L1-enriched Exos at the fractured sites exhibited a negative regulation on T cell activation in the nearby peripheral lymphatic tissues (Fig. 7E–H; Fig. S4).

4. Discussion

Taken together, our results suggest that exosomal PD-L1 coupling to PD-1 on the T cell surface, which significantly accelerated fracture healing in mice. We also demonstrate that Exos carrying active factors can be embedded into a novel hydrogel applied locally to the fracture sites, providing a new potential for enhancing tissue repair and regeneration through immunotherapy.

An overactive inflammatory phase is characterized by continued release of cytotoxic enzymes, inflammatory mediators, and free radicals that cause extensive tissue injury [30]. It has been suggested that suppression of the inflammatory response can enhance callus formation and accelerate fracture healing [31]. The PD-L1/PD-1 immune checkpoint is capable of transmitting inhibitory signals and preventing T cell proliferation [20,21,32]. In the present research, we focus on this immune checkpoint during the inflammation phase of fracture healing. Studying the roles of other immune inflammatory transducers, such as CTLA-4/CD80 and IM3-Galectin9, may provide further information on the modulation of fracture healing.

Exos have the ability to cross barriers, such as the cytoplasmic membrane and the blood-brain barrier, making them ideal molecular carriers [33]. Furthermore, due to their natural material transport ability, inherent long-term circulation capacity and excellent biocompatibility, Exos have great potential as drug delivery vehicles [34,35]. In the present research, we successfully embedded exogeneous PD-L1 into HUVECs to construct an enriched concentration of exosomal PD-L1, identifying potential function as a therapeutic alternative in fracture healing. Exos, derived from HUVECs overexpressing PD-L1, exerted a negative regulation in T cell activation.

To minimize the potential infection risk of anti-inflammatory treatments, we utilized various strategies. Firstly, HUVEC$^{PD-L1@Exos}$ mainly target cytotoxic T cells, but not macrophages and neutrophils, which are the main inflammatory cells working against microbial infection after injury during bone remodeling [36]. Furthermore, Exos administration was initiated on the third day post-fracture, as the first three days are important for immune cells to eliminate cell debris and beat against infection. Moreover, the HA/Gel hydrogel allowed sustained delivery of Exos and displayed self-healing properties against microbial infections. However, our murine fracture model has limitations. For example, linear fractures, small bone defects and large bone defects display differences both in physiopathological conditions as well as molecular mechanisms. In addition, in the present research, we constructed a fracture model rather than a chronic bone non-union model, in which the exosomal PD-L1 may exert robust effects in ameliorating the immune inflammatory response. Multiple fracture models would be constructed to investigate the cross-talk between the immune inflammatory response and bone regeneration in the future study.

5. Conclusions

We introduce a novel application of exosomal PD-L1 as an immunosuppressive therapy for fracture healing. Our findings provide the first example of Exos-based activation of the PD-L1/PD-1 immune checkpoint and subsequent enhancement of bone repair and regeneration. This study offers new theoretical evidence and establishes an experimental platform for Exos-based immunotherapy to treat diseases related to an overactive immune response or immune rejection.

Data availability

All data of this study are available within the paper.

CRediT authorship contribution statement

Ze Lin: Conceptualization, Writing-original draft. **Yuan Xiong:**

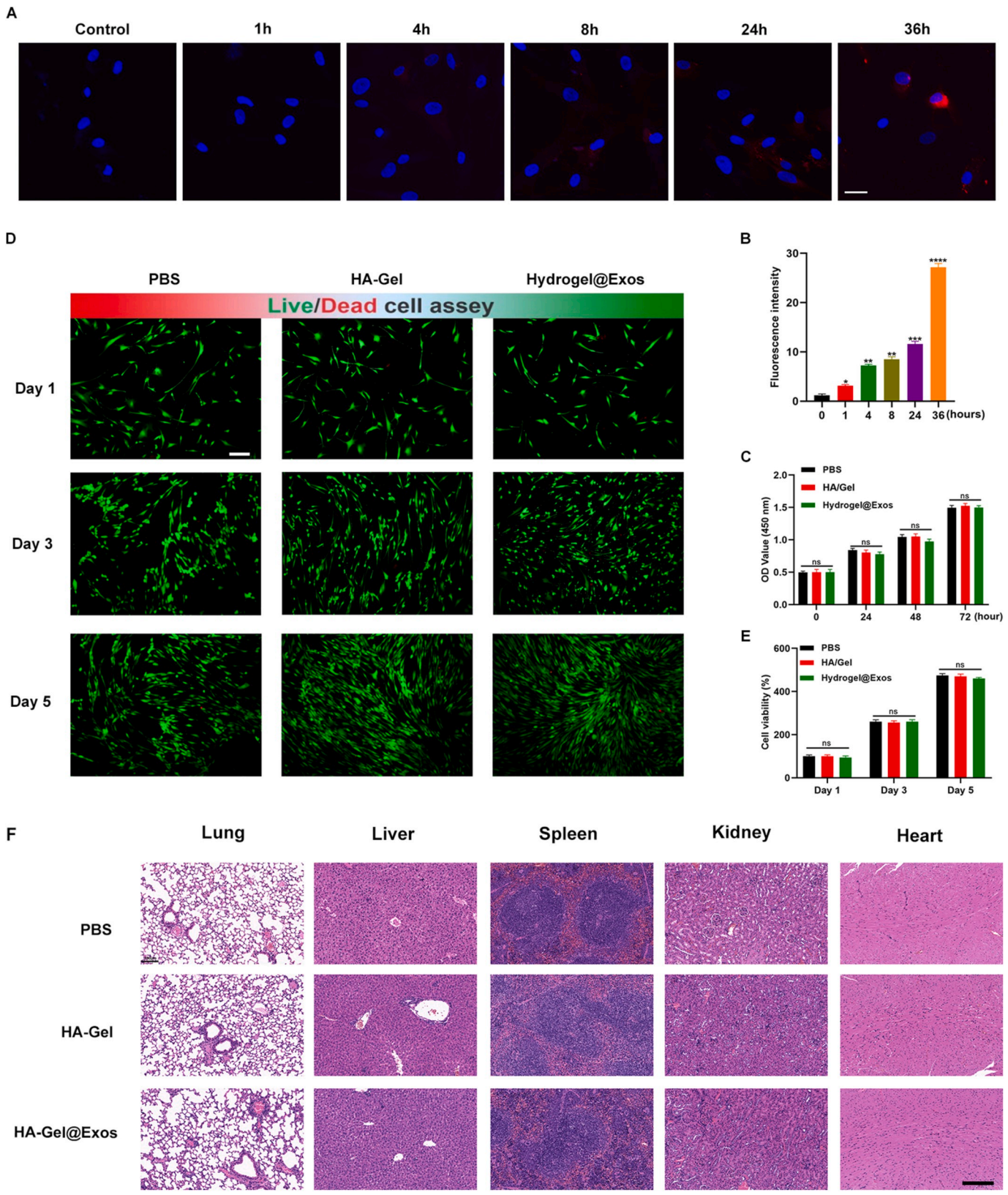

Fig. 5. The release and biocompatible properties of HA/Gel hydrogel. (A) Exos taken up by MSCs, which were cultured with the hydrogel for 0, 1, 4, 8, 24, 36 h. Red, exosomes staining with PKH26. Blue, nuclear staining with DAPI. Scale bar: 5 μm. (B) Quantification of Exos uptake in MSCs was displayed as mean fold changes. n = 3. $^{**}P < 0.01$, $^{***}P < 0.001$. (C) The viability of the cultured MSCs were evaluated by CCK-8 assay. (D-E) The biocompatible properties were observed by live/dead cell staining at 0, 3 and 5 days. (F) H&E staining of the lung, liver, spleen, kidney and heart after administration of PBS, HA-Gel and HA-Gel@Exos for 21 days, scale bar = 100 μm.

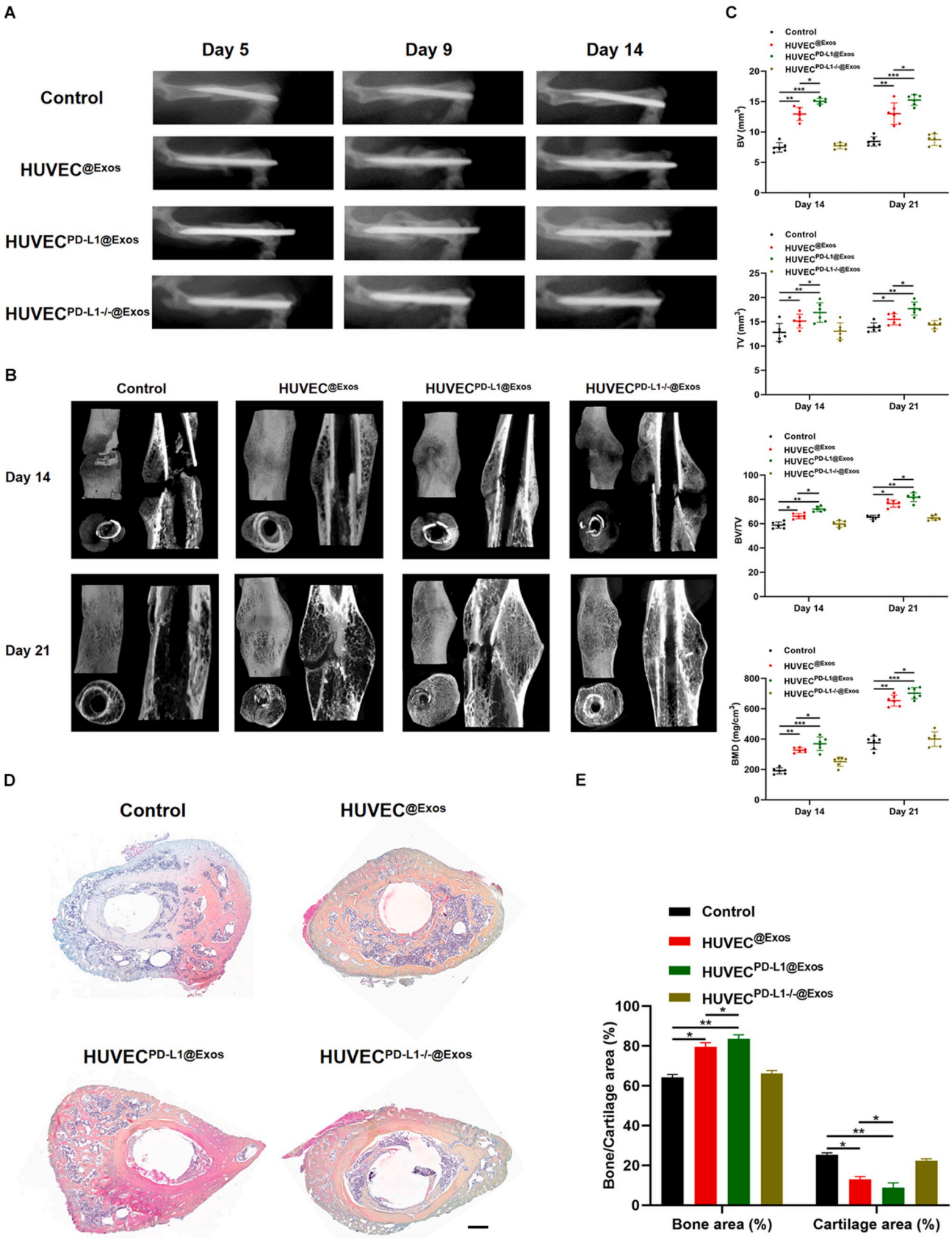

Fig. 6. Exosomal PD-L1 promotes fracture healing in mice. (A) X-rays of fracture repair for Control, HUVEC$^{@Exos}$, HUVEC$^{PD-L1@Exos}$, and HUVEC$^{PD-L1-/-@Exos}$ groups on day 5, 9, and 14 post-injury. (B) Three-dimensional construction and across sections of the fracture site among different treatment groups on day 14 and 21 were constructed by micro-CT. (C) BV, TV, BV/TV, and BMD of the callus on day 14 and 21 post-injury were assessed by micro-CT, n = 6. (D-E) The Alcian Blue/HE/Orange G staining images and corresponding statistical analysis on day 21 post-injury. Scale bar: 500 μm *P < 0.05, **P < 0.01, ***P < 0.001.

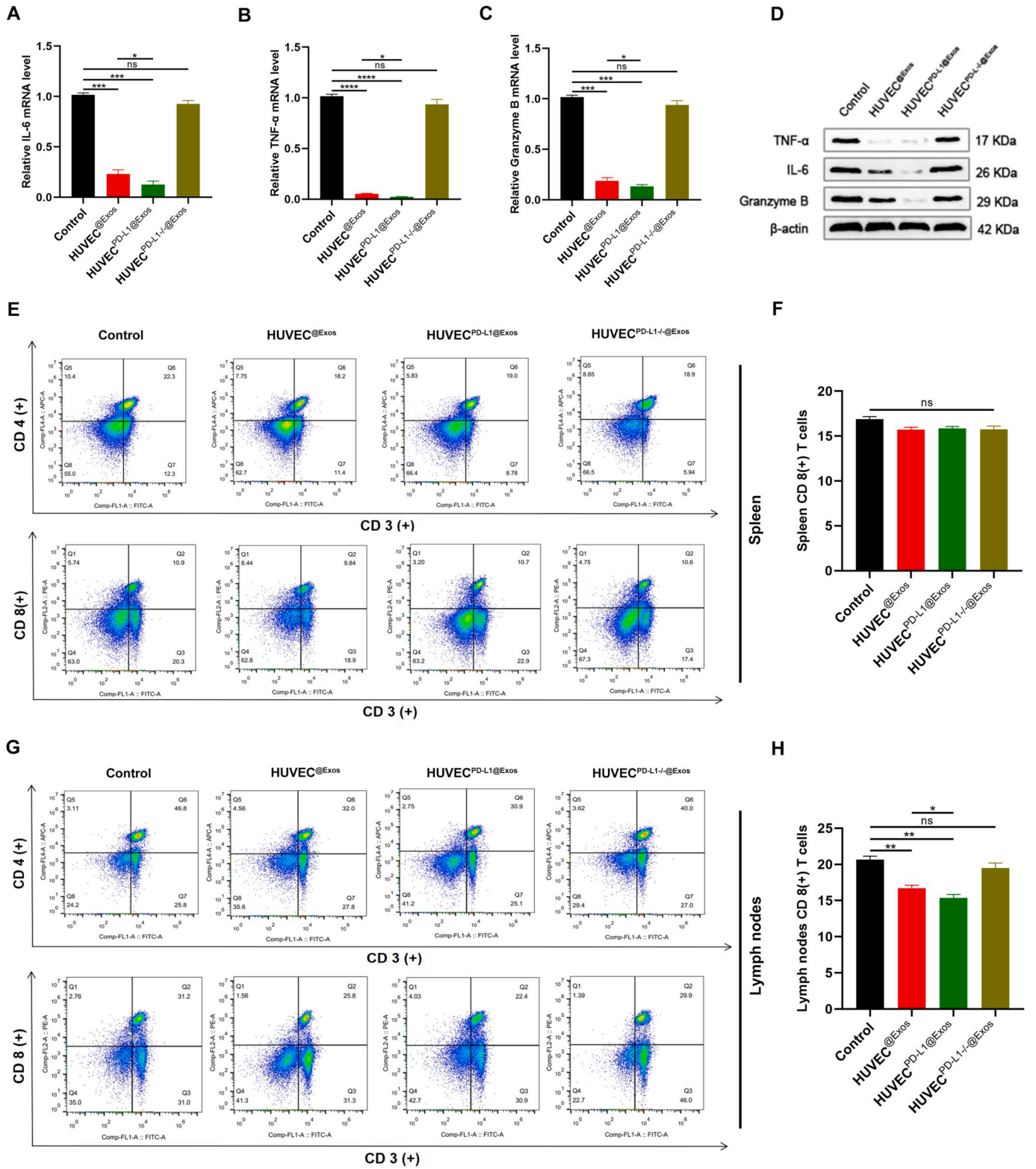

Fig. 7. Exosomal PD-L1 reduces local inflammation at the fracture site. (A-C) The IL-6, TNF-α, and Granzyme B expression in the different treatment groups on 14 days post-fracture were detected by qRT-PCR, n = 3. (D) The expression of IL-6, TNF-α, and Granzyme B were measured by western blot. (E-H) The alteration of CD4(+) and CD8(+) T cells ratio in spleen (E) and lymph nodes (G) were observed by FCM analysis. (F) and (H) are the statistical results of (E) and (G) respectively. *P < 0.05, **P < 0.01.

Investigation, Data curation, Writing-original draft. **Weilin Meng:** Data curation, Writing-original draft. **Yiqiang Hu:** Writing-original draft and revised the manuscript. **Lili Chen:** Revised the manuscript. **Lang Chen:** Investigation and formal analysis. **Hang Xue:** Visualization. **Adriana C. Panayi:** Made critical contributions to the concept and writing of the manuscript, revised the manuscript. **Wu Zhou:** Validation. **Yun Sun:** Technical assistance. **Faqi Cao:** Formal analysis. **Guodong Liu:** Investigation. **Liangcong Hu:** Data collection. **Chenchen Yan:**:Validation.

Xudong Xie: Formal analysis. **Chuanchuan Lin:** Visualization. **Kaiyong Cai:** Investigation and resources. **Qian Feng:** Supervision and validation. **Bobin Mi:** Conception, revised the manuscript. **Guohui Liu:** Conception, supervision, and writing-original draft.

Declaration of competing interest

The authors declare that they have no known competing financial interests or personal relationships that could have appeared to influence the work reported in this paper.

Acknowledgements

This work was supported by the National Science Foundation of China (No. 82002313, No. 82072444, 31900963), Hubei Province Key Laboratory of Oral and Maxillofacial Development and Regeneration (No.2020kqhm008), the Health Commission of Hubei Province (No. WJ2019Z009), the Wuhan Union Hospital "Pharmaceutical Technology nursing" special fund (No. 2019xhyn021), and the China Postdoctoral Science Foundation (No. 2021TQ0118).

Appendix A. Supplementary data

Supplementary data to this article can be found online at https://doi.org/10.1016/j.bioactmat.2021.10.042.

References

[1] C. Wang, J. Ying, X. Nie, T. Zhou, D. Xiao, G. Swarnkar, Y. Abu-Amer, J. Guan, J. Shen, Bone Res. 9 (1) (2021) 29, https://doi.org/10.1038/s41413-021-00150-4.
[2] Y. Wang, S. Shen, T. Hu, G.R. Williams, Y. Bian, B. Feng, R. Liang, X. Weng, ACS Nano 15 (6) (2021) 9732–9745, https://doi.org/10.1021/acsnano.1c00461.
[3] B. Mi, Y. Xiong, L. Chen, C. Yan, Y. Endo, Y. Liu, J. Liu, L. Hu, Y. Hu, Y. Sun, F. Cao, W. Zhou, G. Liu, Aging (Albany NY) 11 (24) (2019) 11988–12001, https://doi.org/10.18632/aging.102524.
[4] A. Bardos, S. Sabhrawal, G. Tytherleigh-Strong, Orthop. J. Sports Med. 9 (6) (2021), https://doi.org/10.1177/23259671211010804, 23259671211010804.
[5] M. Abdelkhalek, B.S. El-Alfy, A.M. Ali, Int. Orthop. (2021), https://doi.org/10.1007/s00264-021-05078-2.
[6] M. Sabaté-Brescó, C.M. Berset, S. Zeiter, B. Stanic, K. Thompson, M. Ziegler, R. G. Richards, L. O'Mahony, T.F. Moriarty, Biol. Open (2021), https://doi.org/10.1242/bio.057315.
[7] R.L.-Y. Shin, C.-W. Lee, O.Y.-J. Shen, H. Xu, O.K.-S. Lee, Stem Cell. Int. 2021 (2021) 8835156, https://doi.org/10.1155/2021/8835156.
[8] P. Qiu, M. Li, K. Chen, B. Fang, P. Chen, Z. Tang, X. Lin, S. Fan, Biomaterials 227 (2020) 119552, https://doi.org/10.1016/j.biomaterials.2019.119552.
[9] Y. Zhu, K. Zhang, R. Zhao, X. Ye, X. Chen, Z. Xiao, X. Yang, X. Zhu, K. Zhang, Y. Fan, X. Zhang, Biomaterials 147 (2017) 133–144, https://doi.org/10.1016/j.biomaterials.2017.09.018.
[10] B. Mi, L. Chen, Y. Xiong, C. Yan, H. Xue, A.C. Panayi, J. Liu, L. Hu, Y. Hu, F. Cao, Y. Sun, W. Zhou, G. Liu, J. Nanobiotechnol. 18 (1) (2020) 68, https://doi.org/10.1186/s12951-020-00624-3.
[11] Y. Xiong, L. Chen, C. Yan, W. Zhou, Y. Endo, J. Liu, L. Hu, Y. Hu, B. Mi, G. Liu, Small 16 (3) (2020), e1904044, https://doi.org/10.1002/smll.201904044.
[12] D. Wu, S. Deng, L. Li, T. Liu, T. Zhang, J. Li, Y. Yu, Y. Xu, Cell Death Dis. 12 (8) (2021) 721, https://doi.org/10.1038/s41419-021-04004-z.
[13] Y. Xiong, L. Chen, C. Yan, W. Zhou, T. Yu, Y. Sun, F. Cao, H. Xue, Y. Hu, D. Chen, B. Mi, G. Liu, J. Nanobiotechnol. 18 (1) (2020) 66, https://doi.org/10.1186/s12951-020-00622-5.
[14] Z. Zhuo, J. Wang, Y. Luo, R. Zeng, C. Zhang, W. Zhou, K. Guo, H. Wu, W. Sha, H. Chen, Acta Biomater. (2021), https://doi.org/10.1016/j.actbio.2021.07.027.
[15] M. Monguió-Tortajada, C. Prat-Vidal, M. Moron-Font, M. Clos-Sansalvador, A. Calle, P. Gastelurrutia, A. Cserkoova, A. Morancho, M.Á. Ramírez, A. Rosell, A. Bayes-Genis, C. Gálvez-Montón, F.E. Borràs, S. Roura, Bioact. Mater. 6 (10) (2021) 3314–3327, https://doi.org/10.1016/j.bioactmat.2021.02.026.
[16] L. Fan, P. Guan, C. Xiao, H. Wen, Q. Wang, C. Liu, Y. Luo, L. Ma, G. Tan, P. Yu, L. Zhou, C. Ning, Bioact. Mater. 6 (9) (2021) 2754–2766, https://doi.org/10.1016/j.bioactmat.2021.02.005.
[17] Y. Enomoto, P. Li, L.M. Jenkins, D. Anastasakis, G.C. Lyons, M. Hafner, W. J. Leonard, Cancer Gene Ther. (2021), https://doi.org/10.1038/s41417-021-00352-2.
[18] F. Cichocki, R. Bjordahl, S. Gaidarova, S. Mahmood, R. Abujarour, H. Wang, K. Tuininga, M. Felices, Z.B. Davis, L. Bendzick, R. Clarke, L. Stokely, P. Rogers, M. Ge, M. Robinson, B. Rezner, D.L. Robbins, T.T. Lee, D.S. Kaufman, B.R. Blazar, B. Valamehr, J.S. Miller, Sci. Transl. Med. 12 (568) (2020), https://doi.org/10.1126/scitranslmed.aaz5618.
[19] S.S. Badve, F. Penault-Llorca, J.S. Reis-Filho, R. Deurloo, K.P. Siziopikou, C. D'Arrigo, G. Viale, J. Natl. Cancer Inst. (2021), https://doi.org/10.1093/jnci/djab121.
[20] N. Ioannou, P.R. Hagner, M. Stokes, A.K. Gandhi, B. Apollonio, M. Fanous, D. Papazoglou, L.-A. Sutton, R. Rosenquist, R.-M. Amini, H. Chiu, A. Lopez-Girona, P. Janardhanan, F.T. Awan, J. Jones, N.E. Kay, T.D. Shanafelt, M.S. Tallman, K. Stamatopoulos, P.E.M. Patten, A. Vardi, A.G. Ramsay, Blood 137 (2) (2021) 216–231, https://doi.org/10.1182/blood.2020006073.
[21] Z. Xu, H.-I. Tsai, Y. Xiao, Y. Wu, D. Su, M. Yang, H. Zha, F. Yan, X. Liu, F. Cheng, H. Chen, ACS Nano 14 (7) (2020) 7959–7969, https://doi.org/10.1021/acsnano.9b09065.
[22] M.Z. Noman, S. Parpal, K. Van Moer, M. Xiao, Y. Yu, J. Viklund, A. De Milito, M. Hasmim, M. Andersson, R.K. Amaravadi, J. Martinsson, G. Berchem, B. Janji, Sci. Adv. 6 (18) (2020), eaax7881, https://doi.org/10.1126/sciadv.aax7881.
[23] W.-J. Chen, X.-F. Hu, M. Yan, W.-Y. Zhang, X.-B. Mao, Y.-W. Shu, Atherosclerosis 244 (2016) 108–112, https://doi.org/10.1016/j.atherosclerosis.2015.11.002.
[24] H. Song, X. Li, Z. Zhao, J. Qian, Y. Wang, J. Cui, W. Weng, L. Cao, X. Chen, Y. Hu, J. Su, Nano Lett. 19 (5) (2019) 3040–3048, https://doi.org/10.1021/acs.nanolett.9b00287.
[25] D. Su, H.-I. Tsai, Z. Xu, F. Yan, Y. Wu, Y. Xiao, X. Liu, Y. Wu, S. Parvanian, W. Zhu, J.E. Eriksson, D. Wang, H. Zhu, H. Chen, F. Cheng, J. Extracell. Vesicles 9 (1) (2019) 1709262, https://doi.org/10.1080/20013078.2019.1709262.
[26] Y. Xiong, C. Yan, L. Chen, Y. Endo, Y. Sun, W. Zhou, Y. Hu, L. Hu, D. Chen, H. Xue, B. Mi, G. Liu, J. Cell Mol. Med. 24 (1) (2020) 1076–1086, https://doi.org/10.1111/jcmm.14832.
[27] B. Mi, Y. Xiong, C. Yan, L. Chen, H. Xue, A.C. Panayi, L. Hu, Y. Hu, W. Zhou, F. Cao, G. Liu, J. Cell Mol. Med. 24 (11) (2020) 6385–6396, https://doi.org/10.1111/jcmm.15284.
[28] G. Ma, C. Li, Z. Zhang, Y. Liang, Z. Liang, Y. Chen, L. Wang, D. Li, M. Zeng, W. Shan, H. Niu, Front. Oncol. 11 (2021) 697894, https://doi.org/10.3389/fonc.2021.697894.
[29] H. Zheng, Y. Ning, Y. Zhan, S. Liu, Q. Wen, S. Fan, Int. J. Biol. Sci. 17 (10) (2021) 2537–2547, https://doi.org/10.7150/ijbs.60114.
[30] Y. Xiong, L. Chen, T. Yu, C. Yan, W. Zhou, F. Cao, X. You, Y. Zhang, Y. Sun, J. Liu, H. Xue, Y. Hu, D. Chen, B. Mi, G. Liu, Aging (Albany NY) 12 (10) (2020) 8968–8986, https://doi.org/10.18632/aging.103143.
[31] Y. Sun, Y. Xiong, C. Yan, L. Chen, D. Chen, B. Mi, G. Liu, Am. J. Transl. Res. 11 (8) (2019) 4746–4760.
[32] D. Sugiura, T. Maruhashi, I.-M. Okazaki, K. Shimizu, T.K. Maeda, T. Takemoto, T. Okazaki, Science 364 (6440) (2019) 558–566, https://doi.org/10.1126/science.aav7062.
[33] Y. Hu, R. Tao, L. Chen, Y. Xiong, H. Xue, L. Hu, C. Yan, X. Xie, Z. Lin, A.C. Panayi, B. Mi, G. Liu, J. Nanobiotechnol. 19 (1) (2021) 150, https://doi.org/10.1186/s12951-021-00894-5.
[34] G.C. Terstappen, A.H. Meyer, R.D. Bell, W. Zhang, Nat. Rev. Drug Discov. 20 (5) (2021) 362–383, https://doi.org/10.1038/s41573-021-00139-y.
[35] A. Robson, Nat. Rev. Cardiol. 18 (3) (2021) 150–151, https://doi.org/10.1038/s41569-020-00498-w.
[36] L.C. Hofbauer, A. Bozec, M. Rauner, F. Jakob, S. Perner, K. Pantel, Nat. Rev. Clin. Oncol. 18 (8) (2021) 488–505, https://doi.org/10.1038/s41571-021-00499-9.